

# Water splitting on metastable catalysts

Nathalie Vonrüti and Ulrich Aschauer

Department of Chemistry and Biochemistry, University of Bern, Freiestrasse 3, CH-3012 Bern, Switzerland

(Dated: December 14, 2024)

The oxygen evolution reaction has been widely studied for electrochemical and photocatalytic water-splitting. While most computational studies have focused on materials with stable surfaces for which the overpotential can be readily computed, we determine here, using density functional theory calculations, free energy profiles for the oxygen evolution reaction on defective (001) surfaces of the metastable oxynitride  $\text{LaTiO}_2\text{N}$ , the metastable  $d^4$  oxide  $\text{SrRuO}_3$  and the stable  $d^0$  oxide  $\text{SrTiO}_3$ . For all three we find large differences in overpotentials for various reaction sites on different defective surfaces. The computed overpotentials generally follow the universal scaling relations and we find for all three materials several reaction sites with an overpotential close to the top of the activity volcano. This implies that metastability-induced dissolution could strongly enhance the activity of metastable catalysts.

## I. INTRODUCTION

Hydrogen production by (photo)electrochemical water splitting has been intensively studied as a route to convert electrical or solar energy to chemical energy. The bottleneck in this process is the oxygen evolution reaction (OER), which was computationally investigated for different material classes such as metals<sup>1</sup> and oxides<sup>2</sup>. In these studies the reaction mechanism consists of four consecutive one-electron transfer steps with reaction intermediates being  $\ast\text{OH}$ ,  $\ast\text{O}$  and  $\ast\text{OOH}$ . It was shown that the binding energies of these species are connected through scaling relations, suggesting that there is only one independent parameter that determines the free energy profile of the OER and thus the activity of the catalyst<sup>1-3</sup>.

While many computational studies compare the activity of stoichiometric low-index<sup>4</sup> and ideal oxidized<sup>5</sup> surfaces of different oxides, there are only a few studies that report the theoretical activity for reaction sites in the vicinity of point defects, steps or kinks<sup>6,7</sup>. While a defect-free stoichiometric surface should be a good approximation for a stable material, several experiments indicate an inverse correlation between the activity and the stability of heterogeneous OER catalysts<sup>8,9</sup>. For a catalyst that is thermodynamically unstable under OER conditions but shows metastability due slow dissolution kinetics, we do not expect a static, thermodynamically determined surface with a single reaction site and therefore a single activity but rather a dynamic surface with a variety of different reaction sites and corresponding activities. The description of such metastable materials by defect-free stoichiometric surface is certainly less valid as the experimentally measured activity is affected by dissolution kinetics as discussed for the case of  $\text{RuO}_2$ <sup>7</sup>.

The aim of the present work is to obtain a computational description of the OER on the surfaces of metastable materials. To account for the metastability, we will study the OER on a large variety of different reaction sites by sampling a large number of defective surface configurations. While electrochemical water splitting has mainly been investigated for oxide catalysts,

oxynitrides hold more promise for solar water splitting as the higher lying nitrogen  $2p$  states decrease the band gap and lead to an improved light absorption compared to oxides. We will therefore compare the metastable oxynitride  $\text{LaTiO}_2\text{N}$ <sup>10</sup> and the metastable oxide  $\text{SrRuO}_3$ <sup>11,12</sup>. Since these two materials differ - besides their anion composition - also in their  $d$  electron count we will additionally study  $\text{SrTiO}_3$  which is not unstable but a  $d^0$  oxide thus making it possible to deduce if our observations originate from the anion composition or the  $d$  electron count and the resulting metallic/insulating nature of the catalyst.

## II. METHODS

While  $\text{LaTiO}_2\text{N}$  assumes a *cis* anion order in the bulk to maximize the overlap between the N  $2p$  and the Ti  $3d$  orbitals<sup>13</sup>, a *trans* anion order was predicted for the (001) surface as it cancels polarity<sup>14</sup>. We therefore perform calculation on this *trans* surface but to account for the metastability also investigate the OER for the *cis* ordered surface, which is likely to become the exposed termination as the dissolution proceeds. However, for simplicity, we do not distinguish between them in the results section as we did not find any differences between the two anion orders. For all three materials we investigate both the AO and  $\text{BO}_2$  terminated surface, always assuming that for a metastable or unstable material both terminations are exposed.

Our stoichiometric and clean surface slab models contain four surface cation sites and we create between one and four nitrogen, titanium, ruthenium, lanthanum or strontium vacancies in the top layer of the surface to obtain defective surfaces (see figure 1 for an example). We do not explicitly consider oxygen vacancies, since these are unlikely to form under oxidizing OER conditions<sup>5</sup>. Occasionally, during surface relaxation - in particular for high cation vacancy concentrations - either  $\text{O}_2$  or  $\text{N}_2$  recombines and desorbs. In these cases we stop the calculation and remove the desorbed molecules before continuing the calculation, which can in effect lead to oxygen

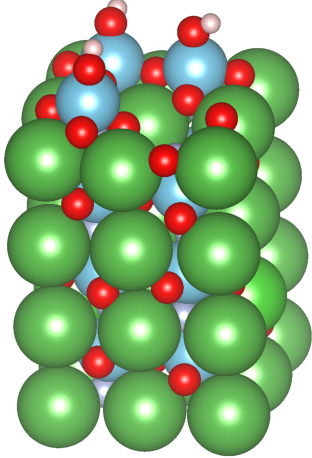
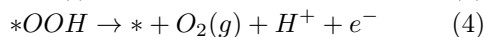
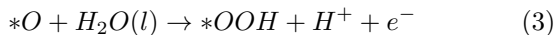
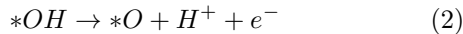
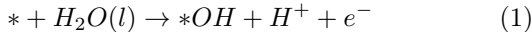


FIG. 1: Sketch of a *trans* LaTiO<sub>2</sub>N slab with one Ti vacancy and the Ti atoms in the top layer covered with OH. (Color code: La = green, Ti = blue, O = red, H = white). Structure visualized using VESTA<sup>15</sup>.

vacancies. Since potentials relevant for photocatalytic water splitting often lead to formation of oxidising surface species<sup>5</sup>, we also cover surface metal sites with either OH or O in top position in the case of Ti and Ru as well as in the bridge position for La and Sr.

For these surfaces we calculate the OER free energy profile on symmetrically inequivalent titanium, ruthenium, lanthanum and strontium reaction sites in the top-most formula-unit layer - meaning for example that for a defective BO<sub>2</sub> terminated surface also an A atom could become the reaction site. Due to a progressive loss in structure with increasing defect density, we also include configurations where oxygen sites that are part of the slab participate in the OER (see figure 2 b). This so-called lattice oxygen evolution was experimentally observed<sup>16-18</sup> and also explained by basic thermodynamic concepts<sup>19</sup>. While different lattice oxygen evolution mechanisms have been proposed<sup>20,21</sup>, we investigate in this study only the one shown in figure 2b), which is mathematically equivalent to the conventional mechanism shown in figure 2a) but operates on an oxygen deficient surface. We can thus describe both reactions by four proton coupled electron transfer (PCET) steps with \* indicating the reaction site:



In total we calculate the OER on 770 symmetrically inequivalent reaction sites (327 *trans* LaTiO<sub>2</sub>N, 135 *cis* LaTiO<sub>2</sub>N, 176 SrTiO<sub>3</sub>, 132 SrRuO<sub>3</sub>) on 106 LaTiO<sub>2</sub>N, 35 SrTiO<sub>3</sub> and 39 SrRuO<sub>3</sub> (001) defective surface models. The larger number of reaction sites on the oxyni-

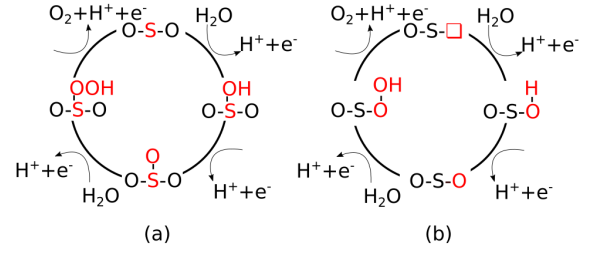


FIG. 2: a) The conventional oxygen evolution mechanism and b) one possible lattice oxygen evolution mechanism.

tride stems from anion-induced symmetry breaking. For roughly  $2/3$  of the reaction sites either of the \*OOH and \*OH intermediates was not stable or the reaction site changed during structural relaxation and we exclude these cases from our analysis.

We calculated the change in free energy ( $\Delta G$ ) of the above four reactions using the computational standard hydrogen electrode (SHE)<sup>22</sup>, where the energy of a proton and an electron equals half the energy of a hydrogen molecule. As the theoretical overpotential is not dependent on the pH or the potential<sup>2</sup> we perform our calculations at standard conditions (pH=0, T=298.15K) and U=0. Zero point energies (ZPE) and entropies (S) of the reaction intermediates were included as detailed elsewhere<sup>23</sup>. In contrast to other studies where ZPE was calculated for reaction intermediates in different environments (bridge vs. top site)<sup>23</sup>, we always use the ZPE at the top site. Given that for defective surfaces a full ZPE evaluation would be computationally prohibitively expensive and that previously reported changes in ZPE were minor<sup>23</sup>, this approach will yield correct trends for defective surfaces.

We estimate the activity of a specific reaction site by the largest step in its OER free energy profile:

$$\Delta G^{OER} = \max[\Delta G_1^0, \Delta G_2^0, \Delta G_3^0, \Delta G_4^0], \quad (5)$$

$\Delta G_{1-4}^0$  being the change in free energy of the four OER steps (equations 1 - 4). The calculated overpotential is given by:

$$\eta^{OER} = (\Delta G^{OER}/e) - 1.23V \quad (6)$$

where 1.23V is the potential needed to make all  $\Delta G$ s equal to zero for an ideal catalyst. The adsorption free energies of the intermediate species  $\Delta G_O$ ,  $\Delta G_{OH}$  and  $\Delta G_{OOH}$  were calculated as follows:

$$\Delta G_{ads} = G_{ads+slab} - G_{slab} - nG_{\text{H}_2\text{O}} - mG_{\text{H}_2}, \quad (7)$$

where free energies include changes in ZPE and S while n and m are stoichiometric coefficients that preserve the number of atoms on both sides of the respective reaction.

We further compare the calculated overpotential  $\eta^{OER}$  with the overpotential  $\eta_{UD}^{OER}$  predicted by the unique

descriptor  $\Delta G_2^0$ : It was established that there exists a universal scaling relation between the adsorption energies of the reaction intermediates  $^*\text{OH}$  and  $^*\text{OOH}$ , their difference being a constant of approximately 3.2 eV for metal and oxide surfaces irrespective of the reaction site<sup>24</sup>. Since the overpotential for oxides and metals is generally determined by either step 2 ( $\Delta G_2^0$ ) or 3 ( $\Delta G_3^0 = 3.2 \text{ eV} - \Delta G_2^0$ ) of the OER, the former is often a suitable unique descriptor of the OER activity that determines the overpotential<sup>2</sup>:

$$\eta_{UD}^{OER} = \max[\Delta G_2^0, 3.2 \text{ eV} - \Delta G_2^0]/e - 1.23 \text{ V} \quad (8)$$

with

$$\Delta G_2^0 = \Delta G_O - \Delta G_{OH} \quad (9)$$

Under the assumption of an optimal  $\Delta G_2^0 = \Delta G_3^0 = 1/2 \cdot 3.2 \text{ eV} = 1.6 \text{ eV}$ , one arrives at a minimum possible overpotential of  $1.6 \text{ eV}/e - 1.23 \text{ V} = 0.37 \text{ V}$ . Deviations of  $\Delta G_2^0$  from this ideal value lead to larger overpotentials.

We determine energies of the various adsorbate covered surfaces by density functional theory (DFT) calculations using the Quantum ESPRESSO<sup>25</sup> package at the GGA+U level of theory with the PBE<sup>26</sup> exchange-correlation functional and a Hubbard U<sup>27</sup> of 3 eV applied to the titanium 3d states. We do not apply a Hubbard U on ruthenium 4d orbitals as this setup results in the best agreements with experimentally measured magnetic moments and the density of states at the Fermi energy. We use ultrasoft pseudopotentials<sup>28</sup> with La(5s,5p,5d,6s), Sr(4s,4p,5s), Ti(3s,3p,3d,4s), Ru(4d,5s,5p), O(2s,2p) and N(2s,2p) electrons as valence states to describe the interaction between electrons and nuclei and perform spin-polarized calculations in the case of SrRuO<sub>3</sub>. The cutoff for the plane-wave basis set is 40 Ry and 320 Ry for the kinetic energy and the augmented density respectively for LaTiO<sub>2</sub>N and SrTiO<sub>3</sub>, while for SrRuO<sub>3</sub> we use slightly higher cutoffs of 50 Ry and 500 Ry respectively. We start our calculation from a 40-atom pseudo-cubic perovskite cell and create asymmetric 1x1x2 surface slabs (see figure 1) with at least 10 Å vacuum, two fixed atomic layers at the bottom of the slab and a dipole correction in the vacuum layer<sup>29</sup>. The Brillouin zone is sampled with a 4x4x1 Monkhorst-Pack<sup>30</sup> k-point grid for LaTiO<sub>2</sub>N and SrTiO<sub>3</sub> and a 6x6x1 grid for SrRuO<sub>3</sub>. We relax ionic position until forces converge below 0.05 eVÅ<sup>-1</sup> and total energies change by less than  $1.4 \cdot 10^{-5} \text{ eV}$ .

### III. RESULTS AND DISCUSSION

We begin our analysis by comparing the calculated overpotentials  $\eta^{OER}$  with the overpotential determined via the unique descriptor  $\eta_{UD}^{OER}$  and find in general a good agreement for the majority of the calculated overpotentials (see figure 3). Most remarkable is the fact that we find for all three materials a continuous distribution of overpotentials within a large range of the unique descriptor  $\Delta G_2^0$ , including also the top of the volcano. While

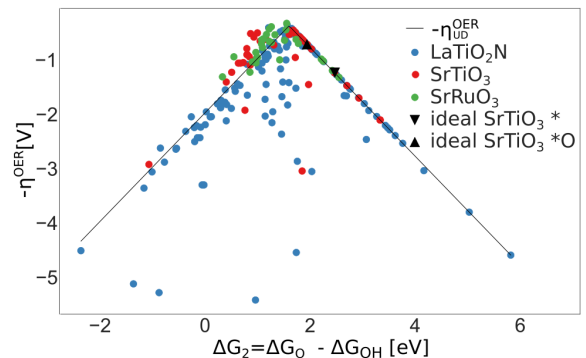


FIG. 3: Volcano plot of LaTiO<sub>2</sub>N, SrTiO<sub>3</sub> and SrRuO<sub>3</sub> and the overpotential  $\eta_{UD}^{OER}$  predicted by the unique descriptor  $\Delta G_2^0$  assuming a binding energy difference of 3.2 eV between the adsorption energy of  $^*\text{OOH}$  and  $^*\text{OH}$ .

we cannot say, which sites (if any) will be predominantly present on a dissolving surface, it seems likely from the large number of sites close to the minimum overpotential, that some of these will at least be transiently present. We therefore postulate that *in operando* surface dissolution can lead to the appearance of highly activate sites, which results in an enhanced apparent activity of the catalyst. Similar conclusion have been drawn for Pt<sub>13</sub> clusters where metastable isomers can contribute to or even dominate the experimentally observed activity<sup>31</sup>. It was also shown experimentally that perovskite oxide electrocatalysts with structural flexibility can lead to superior activity<sup>32</sup>. We want to stress that while this improvement is certainly realistic for the metastable LaTiO<sub>2</sub>N and SrRuO<sub>3</sub>, we do not expect a similar activity enhancement on the stable SrTiO<sub>3</sub> surface, where activities of the stoichiometric surfaces as indicated by black triangles in figure 3 should prevail.

By determining the slope between adsorption energies of the  $^*\text{OH}$  and  $^*\text{OOH}$  intermediates, we find slight deviations from the universal scaling law, which would result in tips of the volcano at slightly smaller overpotentials than 0.37 V for SrTiO<sub>3</sub> ( $\eta^{OER} = 0.23 \text{ V}$ ) and SrRuO<sub>3</sub> ( $\eta^{OER} = 0.26 \text{ V}$ ) and slightly higher for LaTiO<sub>2</sub>N ( $\eta^{OER} = 0.40 \text{ V}$ ). Despite these differences, we do for SrTiO<sub>3</sub> and SrRuO<sub>3</sub> not find actual reaction sites with overpotentials smaller than 0.37 V. In fact, a recent review stressed that breaking the universal scaling relation between  $^*\text{OOH}$  and  $^*\text{OH}$  is a necessary but not sufficient condition to optimize the OER since all four PCET steps need to have equal energy differences to reach zero overpotential<sup>33</sup>. Further, while there are only small differences between both oxides and both show a rather good agreement between the calculated  $\eta^{OER}$  and the unique-descriptor overpotentials  $\eta_{UD}^{OER}$ , we find for LaTiO<sub>2</sub>N a not insignificant number of OERs that show large deviations from  $\eta_{UD}^{OER}$ . For LaTiO<sub>2</sub>N a more detailed analysis of the reaction free energies of the four

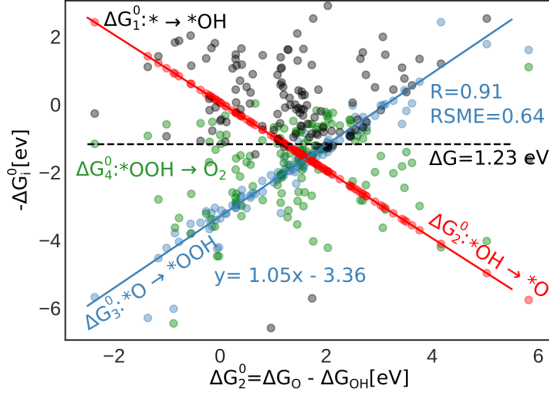


FIG. 4: Negative reaction free energy-dependence of the four charge transfer steps in the OER  $\Delta G_i^0$  on the descriptor  $\Delta G_2^0$  for *trans/cis* LaTiO<sub>2</sub>N. The dashed line indicates the ideal free energy of the four steps (1.23 V). Therefore, the difference between the lowest of the four negative reaction energies of a specific OER and the dashed line represents the predicted overpotential for this OER.

charge transfer steps  $\Delta G_i^0$  (see figure 4), reveals that while for most reactions  $\Delta G_2^0$  or  $\Delta G_3^0$  (blue and red data points) have the largest free-energy change, there are some reactions where  $\Delta G_4^0$  (green data points) lie lower on the y-axis, representing a larger free energy change and thus being the limiting step. This implies that the step from \*OOH to O<sub>2</sub> is energetically less favorable while at the same time the formation of \*OH is more favorable for the oxynitride, which was not observed for oxides<sup>2</sup> and suggests a stronger adsorption of \*OOH on the oxynitride. Especially close to the top of the predicted volcano, this leads to larger calculated overpotentials compared to the unique-descriptor overpotentials  $\eta_{UD}^{OER}$  for some of the OERs. For the metastable materials, we find the lowest overpotentials on B-site deficient surfaces, the OER occurring on one of the remaining B sites. While this suggests that a dissolving BO<sub>2</sub> termination should have a high activity, we can based on our data not comment on the occurrence probability of these particular structures.

From the volcano plot in figure 3 we can see a further difference between the two oxides and the oxynitride: While for the oxynitride the descriptor value  $\Delta G_2^0$  ranges from -2 eV to 6 eV, the two oxides seem to have a much smaller range of  $\Delta G_2^0$  and their overpotentials are therefore more concentrated around the top of the volcano. This raises the question whether this difference between oxides and oxynitrides is due to specific characteristics of the two material classes or simply due to the smaller sample size for oxides. In looking for material parameters that determine and explain the range of the descriptor  $\Delta G_2^0$ , we fail to identify single structural features (such as e.g. reaction site species, angles and bond lengths of

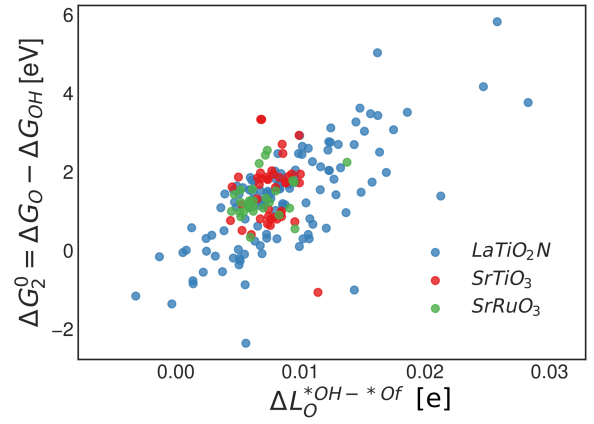


FIG. 5: Correlation between change in oxygen Löwdin charges  $\Delta L_O^{*OH-*O}$  and the descriptor  $\Delta G_2^0$ . Larger  $\Delta L_O^{*OH-*O}$  indicate that the oxygen atoms lose more electrons when the reaction intermediate changes from \*OH to \*O. This is energetically costly and results in large free energy changes  $\Delta G_2^0$ .

reaction intermediates or the adsorbate coverages to mention only a few). We also find no correlation of  $\Delta G_2^0$  with global properties such as the dipole moment of the slab or the nominal charge of the atoms. However, in agreement with other studies<sup>34,35</sup>, we observe a correlation of  $\Delta G_2^0$  with the electronic structure. To characterize the charge transfer towards different reaction intermediates we look at the average Löwdin charges on the O and N atoms. We find the best correlations if we include all N and O atoms and not only surface atoms. We compute differences between element-averaged Löwdin charges for the different reaction steps:

$$\Delta L_a^{i-j} = \frac{1}{N_a^i} \sum_{x \in a} l_x^i - \frac{1}{N_a^j} \sum_{x \in a} l_x^j, \quad (10)$$

where  $a$  is an element (here O or N),  $i$  and  $j$  are two consecutive reaction intermediates,  $N_a^{i/j}$  is the number of  $a$  atoms in the surface structure with the  $i/j$  intermediate and  $l_x^{i/j}$  is the Löwdin charge for atom  $x$  in the structure with intermediate  $i/j$ , while the sum runs over all atoms of element  $a$ .

As we show in figure 5, there is a direct correlation between the descriptor  $\Delta G_2^0$  and the average change in Löwdin charge of the oxygen ions  $\Delta L_O^{*OH-*O}$  for LaTiO<sub>2</sub>N. We do, however, not find a correlation for SrTiO<sub>3</sub> or SrRuO<sub>3</sub>.  $\Delta L_O^{*OH-*O}$  is generally positive meaning that the average Löwdin charge of oxygen is higher for the OH\* than for the O\* intermediate, which we can relate to the fact that oxygen in \*OH attracts electrons from the hydrogen atom and the slab whereas \*O attracts electrons only from the slab. A smaller  $\Delta L_O^{*OH-*O}$  signifies less charge transfers from the slab to the adsorbate during deprotonation, implying that both adsorbates attract a similar number of electrons, which

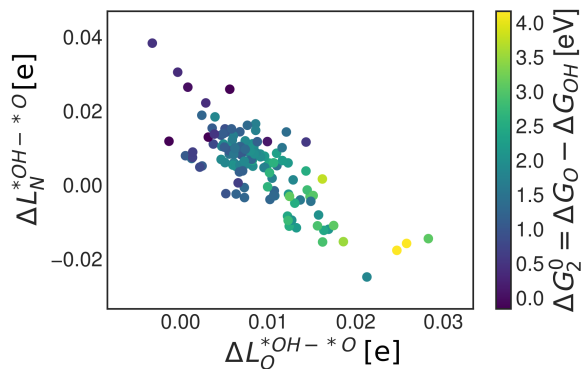


FIG. 6: Correlation between the change in Löwdin charges of nitrogen and oxygen in LaTiO<sub>2</sub>N. The colour bar indicates the value of the descriptor  $\Delta G_2^0$ .

results in an energetically more favorable deprotonation and a smaller  $\Delta G_2^0$ .

For the oxides SrRuO<sub>3</sub> and SrTiO<sub>3</sub> the range of  $\Delta L_O^{*OH-*O}$  is much smaller than for LaTiO<sub>2</sub>N leading to a smaller range in  $\Delta G_2^0$ . We can explain this difference between oxides and oxynitrides by relating the average change in Löwdin charge of oxygen  $\Delta L_O^{*OH-*O}$  to the one of nitrogen  $\Delta L_N^{*OH-*O}$ . As shown in figure 6 we find an inverse correlation between these charge differences, suggesting a charge transfer from N to O. From the color coding of the data points, we see that  $\Delta G_2^0$  is generally smaller when nitrogen loses more electrons (large positive  $\Delta L_N^{*OH-*O}$ ), while the charge change on the oxygen atoms is small. From these observations we propose that nitrogen can act as an electron reservoir: The reaction from \*OH to \*O is favored if nitrogen ions provide electrons, resulting in a lower descriptor value  $\Delta G_2^0$ , while reaction sites, where this charge transfers is not possible result in larger  $\Delta G_2^0$ s. The presence of nitrogen thus explains the wider spread of  $\Delta G_2^0$  and thus the overpotential in oxynitrides compared oxides.

## IV. CONCLUSIONS

In summary, we have shown that the structural variety of reaction sites on dissolving heterogeneous catalysts will, for some sites, lead to overpotentials close to the top of the activity volcano. The observed large spread in overpotentials for just a single reaction mechanism implies that assigning a computed mechanism based on agreement with experimentally measured overpotentials without detailed mechanistic studies is, despite being common practice, highly questionable. Under the assumption that reaction sites with low overpotentials will dominate a catalyst's apparent activity, this implies that instability under electrochemical conditions, such as it occurs for SrRuO<sub>3</sub> and LaTiO<sub>2</sub>N, can indeed enhance the apparent activity.

While we find the unique-descriptor approach to generally work well for these highly defective surfaces, we observe that the strong binding of the \*OOH and \*OH intermediates on LaTiO<sub>2</sub>N can lead to different overpotential-determining steps and larger deviations from the descriptor-based overpotential than for oxides. We find only minor differences in activity between metallic SrRuO<sub>3</sub> and insulating SrTiO<sub>3</sub> but by comparing oxides and oxynitrides, we find that the latter have a much larger spread in descriptor values and hence overpotentials, which we explain with nitrogen acting as an electron reservoir in oxynitride materials.

## V. ACKNOWLEDGEMENTS

This research was funded by the SNF Professorship Grant PP00P2\_157615. Calculations were performed on UBELIX (<http://www.id.unibe.ch/hpc>), the HPC cluster at the University of Bern, the Swiss National Supercomputing Centre (CSCS) under project s766 and SuperMUC at GCS@LRZ, Germany, for which we acknowledge PRACE for awarding us access.

- <sup>1</sup> J. Rossmeisl, A. Logadottir, and J. K. Nørskov, *Chemical physics* **319**, 178 (2005).
- <sup>2</sup> I. C. Man, H.-Y. Su, F. Calle-Vallejo, H. A. Hansen, J. I. Martínez, N. G. Inoglu, J. Kitchin, T. F. Jaramillo, J. K. Nørskov, and J. Rossmeisl, *ChemCatChem* **3**, 1159 (2011).
- <sup>3</sup> J. Rossmeisl, Z.-W. Qu, H. Zhu, G.-J. Kroes, and J. K. Nørskov, *Journal of Electroanalytical Chemistry* **607**, 83 (2007).
- <sup>4</sup> J. H. Montoya, A. D. Doyle, J. K. Nørskov, and A. Vojvodic, *Physical Chemistry Chemical Physics* **20**, 3813 (2018).
- <sup>5</sup> J. H. Montoya, M. Garcia-Mota, J. K. Nørskov, and A. Vojvodic, *Physical Chemistry Chemical Physics* **17**, 2634 (2015).
- <sup>6</sup> C. F. Dickens and J. K. Nørskov, *The Journal of Physical Chemistry C* **121**, 18516 (2017).

- <sup>7</sup> X. Rong and A. M. Kolpak, *The journal of physical chemistry letters* **6**, 1785 (2015).
- <sup>8</sup> S. H. Chang, J. G. Connell, N. Danilovic, R. Subbaraman, K.-C. Chang, V. R. Stamenkovic, and N. M. Markovic, *Faraday Discussions* **176**, 125 (2015).
- <sup>9</sup> N. Danilovic, R. Subbaraman, K.-C. Chang, S. H. Chang, Y. J. Kang, J. Snyder, A. P. Paulikas, D. Strmcnik, Y.-T. Kim, D. Myers, et al., *The Journal of Physical Chemistry Letters* **5**, 2474 (2014).
- <sup>10</sup> I. E. Castelli, K. S. Thygesen, and K. W. Jacobsen, *Topics in Catalysis* **57**, 265 (2014).
- <sup>11</sup> S. H. Chang, N. Danilovic, K.-C. Chang, R. Subbaraman, A. P. Paulikas, D. D. Fong, M. J. Highland, P. M. Baldo, V. R. Stamenkovic, J. W. Freeland, et al., *Nature communications* **5**, 4191 (2014).

- <sup>12</sup> B.-J. Kim, D. F. Abbott, X. Cheng, E. Fabbri, M. Nachttegaal, F. Bozza, I. E. Castelli, D. Lebedev, R. Schäublin, C. Copéret, et al., *ACS Catalysis* **7**, 3245 (2017).
- <sup>13</sup> M. Yang, J. Oró-Solé, J. A. Rodgers, A. B. Jorge, A. Fuertes, and J. P. Attfield, *Nat. Chem.* **3**, 47 (2011).
- <sup>14</sup> S. Ninova and U. Aschauer, *Journal of Materials Chemistry A* **5**, 11040 (2017).
- <sup>15</sup> K. Momma and F. Izumi, *J. Appl. Crystallogr.* **44**, 1272 (2011).
- <sup>16</sup> M. Wohlfahrt-Mehrens and J. Heitbaum, *Journal of electroanalytical chemistry and interfacial electrochemistry* **237**, 251 (1987).
- <sup>17</sup> S. Fierro, T. Nagel, H. Baltruschat, and C. Comninellis, *Electrochemistry Communications* **9**, 1969 (2007).
- <sup>18</sup> O. Diaz-Morales, F. Calle-Vallejo, C. de Munck, and M. T. Koper, *Chemical Science* **4**, 2334 (2013).
- <sup>19</sup> T. Binniger, R. Mohamed, K. Waltar, E. Fabbri, P. Levèque, R. Kötz, and T. J. Schmidt, *Scientific reports* **5**, 12167 (2015).
- <sup>20</sup> A. Grimaud, O. Diaz-Morales, B. Han, W. T. Hong, Y.-L. Lee, L. Giordano, K. A. Stoerzinger, M. T. Koper, and Y. Shao-Horn, *Nature chemistry* **9**, 457 (2017).
- <sup>21</sup> J. S. Yoo, X. Rong, Y. Liu, and A. M. Kolpak, *ACS Catalysis* **8**, 4628 (2018).
- <sup>22</sup> J. K. Nørskov, J. Rossmeisl, A. Logadottir, L. Lindqvist, J. R. Kitchin, T. Bligaard, and H. Jonsson, *The Journal of Physical Chemistry B* **108**, 17886 (2004).
- <sup>23</sup> A. Valdes, Z.-W. Qu, G.-J. Kroes, J. Rossmeisl, and J. K. Nørskov, *The Journal of Physical Chemistry C* **112**, 9872–(2008).
- <sup>24</sup> M. T. Koper, *Journal of Electroanalytical Chemistry* **660**, 254 (2011).
- <sup>25</sup> P. Giannozzi, S. Baroni, N. Bonini, M. Calandra, R. Car, C. Cavazzoni, D. Ceresoli, G. L. Chiarotti, M. Cococcioni, I. Dabo, A. Dal Corso, S. de Gironcoli, S. Fabris, G. Fratesi, R. Gebauer, U. Gerstmann, C. Gougousis, A. Kokalj, M. Lazzeri, L. Martin-Samos, N. Marzari, F. Mauri, R. Mazzarello, S. Paolini, A. Pasquarello, L. Paulatto, C. Sbraccia, S. Scandolo, G. Sclauzero, A. P. Seitsonen, A. Smogunov, P. Umari, and R. M. Wentzcovitch, *J. Phys. Condens. Matter* **21**, 395502 (2009).
- <sup>26</sup> J. P. Perdew, K. Burke, and M. Ernzerhof, *Phys. Rev. Lett.* **77**, 3865 (1996).
- <sup>27</sup> V. I. Anisimov, J. Zaanen, and O. K. Andersen, *Phys. Rev. B* **44**, 943 (1991).
- <sup>28</sup> D. Vanderbilt, *Phys. Rev. B* **41**, 7892 (1990).
- <sup>29</sup> L. Bengtsson, *Physical Review B* **59**, 12301 (1999).
- <sup>30</sup> H. J. Monkhorst and J. D. Pack, *Phys. Rev. B* **13**, 5188 (1976).
- <sup>31</sup> G. Sun and P. Sautet, *Journal of the American Chemical Society* **140**, 2812 (2018).
- <sup>32</sup> E. Fabbri, M. Nachttegaal, T. Binniger, X. Cheng, B.-J. Kim, J. Durst, F. Bozza, T. Graule, R. Schäublin, L. Wiles, et al., *Nature materials* **16**, 925 (2017).
- <sup>33</sup> N. Govindarajan, J. M. García-Lastra, E. J. Meijer, and F. Calle-Vallejo, *Current Opinion in Electrochemistry* (in press).
- <sup>34</sup> A. Vojvodic and J. K. Nørskov, *Science* **334**, 1355 (2011).
- <sup>35</sup> J. K. Nørskov, F. Abild-Pedersen, F. Studt, and T. Bligaard, *Proceedings of the National Academy of Sciences* **108**, 937 (2011).